THERMAL-HYDRAULIC ANALYSIS OF WATER BASED ZrO_2 NANOFLUIDS IN SEGMENTAL BAFFLED SHELL AND TUBE HEAT EXCHANGERS

by

Muhammad SAJJAD[a*], Hassan ALI[b], and Muhammad Sajid KAMRAN[b]

[a] Department of Mechanical Engineering,
Khwaja Fareed University of Engineering and Information Technology, Rahim Yar Khan, Pakistan
[b] Faculty of Mechanical Engineering, University of Engineering and Technology, Lahore, Pakistan

Original scientific paper
https://doi.org/10.2298/TSCI180615291S

Thermal-hydraulic characteristics of water based ZrO_2 nanofluids has been investigated in a segmental baffled shell and tube heat exchanger in turbulent flow regime. The effect of Reynolds number, nanoparticle loading, mass-flow rate, and tube lay-out has been analysed on overall heat transfer coefficient. The effect of Reynolds number on the tube side pressure drop and convective heat coefficient have also been discussed. The effect of shell side mass-flow rate was also investigated on shell side heat transfer coefficient determined using Bell-Delaware method. The nanoparticle volume concentration is taken very low i. e. 0.2%, 0.4%, and 0.8%, respectively. The improvement in both tube side convective heat transfer coefficient and overall heat transfer coefficient has been observed. The maximum improvement in the convective heat transfer coefficient is found to be 14.1% for 0.8% ZrO_2 nanofluids. However, the percentage enhancement in tube side pressure drop was higher than the percentage increment in the tube side heat transfer coefficient.

Key words: *nanofluids, heat exchangers, heat transfer coefficient, pressure drop*

Introduction

Heat exchangers are one of the important potential applications of nanofluids. Nanofluids have acquired a lot of importance in a wide range of applications from last few decades. The nanomaterial, one of the important part of the nanofluid, can be obtained from multiple sources including metals, non-metals, metal oxide, and semiconductors. For example, the metal nanoparticles can be obtained from aluminum, copper and other metals, while metal oxide nanomaterials are obtained from Al_2O_3, TiO_2, CuO, Fe_2O_3, and *etc.* The non-metal nanoparticles, for instance, includes single and multi-walled CNT, graphene oxide, graphene nanoplatelets, and nanodiamonds. The further details on various types of nanparticles, base fluids and nanomaterials along with their thermophysical properties and thermal-hydraulic characteristics can be found in recent review studies performed by Gupta *et al.* [1], Ganvir *et al.* [2], Leong *et al.* [3], and Ambreen and Kim [4].

Farajollahi *et al*. [5] analysed the heat transfer performance of water based Al_2O_3 and TiO_2 nanofluids in a shell and tube heat exchanger. The effect of nanoparticle loading and Peclet number was studied on different parameters such as tube side heat transfer coefficient, tube side Nusselt number, and overall heat transfer coefficient. They observed a maximum

* Corresponding author, e-mail: muhammad.sajjad@kfueit.edu.pk

enhancement in overall heat transfer coefficient of 16% at a volume concentration of 0.75%, and at Peclet number of 50000 for Al_2O_3-water nanofluids. The heat transfer enhancement using multi-walled CNT as a nanomaterial was studied by Lotfi *et al*. [6] in a shell and tube heat exchanger. They observed an increase in the overall heat transfer coefficient with both nanoparticle volume concentrations and flow rate. Cox *et al*. [7] investigated the thermal performance of SiO_2-water nanofluids in shell and tube heat exchanger, considering the effect of mass-flow rate on overall heat transfer coefficient. The maximum intensification in overall heat transfer coefficient was 9% at a weight concentration of 4% and at a mass-flow rate of 950 kg/hr. Albadr *et al*. [8] also investigated the effect of mass-flow rate and volume concentration on thermal characteristics of Al_2O_3-water nanofluids in a shell tube heat exchanger in the turbulent flow regime. The enhancement observed in the overall heat transfer coefficient, was 57% at a volume concentration of 2%.

Akhtari *et al*. [10] carried experimental and CFD analysis to study the heat transfer characteristics of Al_2O_3-water nanofluids in a shell and tube, and in a double pipe heat exchanger. They found significant enhancement in heat transfer coefficient, up to 23.9% at a volume concentration of 0.5%. Shahrul *et al*. [13] analysed the effect of volume concentration on thermophysical properties, heat transfer coefficient, and energy effectiveness of various nanofluids in a shell and tube heat exchanger. The highest improvement in convective heat transfer coefficient was 14.29%, 12.89%, 10.10%, 9.86%, 9.76%, and 2.18% for Al_2O_3, Fe_3O_4, TiO_2, ZnO, CuO, and SiO_2 nanofluids, respectively, at a volume concentration of 0.3% and a mass-flow rate of 50 kg per minute for both shell side and tube side fluid. Kumar and Sonawane [11] experimentally measured the heat transfer performance of nanofluids, prepared by suspending Fe_2O_3 nanoparticles in two types of base fluids *i. e.* water and ethylene glycol. They observed a 20% improvement in the convective heat transfer coefficient for Fe_2O_3-water nanofluids and 13% for Fe_2O_3-EG nanofluids. Shahrul *et al.* [9] experimentally evaluated the performance of three types of nanofluids: Al_2O_3-water, SiO_2-water, and ZnO-water. They found 12% enhancement in overall heat transfer coefficient for 0.5 vol.% SiO_2-water nanofluids, 26% for 0.5 vol.% Al_2O_3-water nanofluids, and 35% for 0.3 vol.% ZnO-water nanofluids, respectively. Heydari *et al.* [14] performed simulations to measure the heat transfer coefficient and heat transfer rate of a number of nanofluids using water and ethylene glycol as a base fluid and taking Al_2O_3, Fe_2O_3, SiO_2, Au, Fe, CuO, and Cu as nanoparticles with volume concentrations of 1-5%. The observed that the heat transfer coefficient decreases with the increase in volume concentration for all types of nanofluids. Haque *et al*. [12] experimentally found maximum enhancement of 35.82% and 59.08% in heat transfer rate and heat transfer coefficient, respectively, for 2 wt.% Al_2O_3-water nanofluids, in a vertical shell and tube heat exchanger. The summary of these important studies can be found in tab. 1. It can be observed from the literature survey that the nanofluids containing ZrO_2 nanoparticles have not extensively been studied in shell and tube heat exchangers. Therefore, the current study investigates the thermal-hydraulic characteristics of water based ZrO_2 nanofluids in a segmental baffled shell and tube heat exchanger.

Heat exchanger specifications

The shell and tube heat exchanger consists of 48 tubes, with an inner and outer diameter of 0.005 m and 0.006 m, respectively. The shell inside and outside diameter are 0.071 m and 0.0748 m, respectively. The tubes are made of brass, and a shell of stainless steel. The heat exchanger consists of three segmental baffles with baffle cut of 30%. The length of the tubes is taken 0.202 m and tube lay-out is 30° unless specified. The hot and cold fluids (*i. e*. nanofluid) were taken on the shell side and tubes side, respectively.

Table 1. Summary of literature survey for the thermal performance of nanofluids in shell and tube heat exchangers

Author(s)	Nanofluids	Particle loading	Findings
Farajollahi *et al*. [5]	Al_2O_3-water	ϕ_v = 0.3-2%	Highest enhancement in overall heat transfer coefficient for H_2O-γ -Al_2O_3 nanofluids was 16% at ϕ_v = 0.75% and Pe = 50000
	TiO_2-water	ϕ_v = 0.15-0.75%	Highest enhancement in overall heat transfer coefficient for TiO_2 -water nanofluids was 24% at ϕ_v = 0.3% and Pe = 44000
Cox *et al.* [7]	SiO_2-water	ϕ_w = 2-6%	Maximum enhancement in total heat transfer coefficient was 9% at ϕ_v = 4% and m = 950 kg/hr
Albadr *et al*. [8]	Al_2O_3-water	ϕ_v = 0.3-2%	Maximum enhancement in overall heat transfer coefficient was 57% at ϕ_v = 2% and Re = 180349.123
Shahrul *et al*. [9]	SiO_2-water	ϕ_v = 0.5%	12% enhancement in overall heat transfer coefficient for 0.5 vol.% SiO_2 -water nanofluids, 26% for 0.5 vol.% Al_2O_3 -water nanofluids, and 35% for 0.3 vol.% ZnO -water nanofluids, respectively
	Al_2O_3-water	ϕ_v = 0.5%	
	ZnO-water	ϕ_v = 0.3%	
Akhtari *et al*. [10]	Al_2O_3-water	ϕ_v = 0.2-0.5%	Enhancement in overall heat transfer coefficient was 23.9% at ϕ_v = 0.5% and base fluid-flow rate of 90 ph
Kumar and Sonawane [11]	Fe_2O_3-water EG-Fe_2O_3	ϕ_v = 0.02-0.08%	Maximum enhancement of 20% for Fe_2O_3/H_2O nanofluids, and 13% for Fe_2O_3/EG nanofluids in convective heat transfer coefficient
Haque *et al*. [12]	Al_2O_3-water	ϕ_m = 1-2%	Maximum improvement in convective heat transfer coefficient was 59.08% for 2 wt.% Al_2O_3 nanofluids

Thermophysical properties of nanofluids

The thermophysical properties of the base fluid and the nanofluids were evaluated at mean temperature for further calculations. The viscosity, thermal conductivity, specific heat capacity and density of water was determined by the correlations of Popiel and Wojtkowiak [15]. The thermophysical properties of ZrO_2 nanofluids were determined, employing eqs. (1) and (4) [16]. The density and specific heat capacity of ZrO_2 nanoparticle were considered 5570 kg/m^3 and 480 kJ/kg K, respectively [17]:

$$\rho_{nf} = \phi_v \rho_{nm} + (1-\phi_v)\rho_{bf} \tag{1}$$

$$\rho_{nf} C_{p,nf} = \phi_v \rho_{nm} C_{p,nm} + (1-\phi_v)\rho_{bf} C_{p,bf} \tag{2}$$

$$\mu_{nf} = \mu_{bf}(550.82\phi_v^2 + 46.801\phi_v + 1) \tag{3}$$

$$k_{nf} = k_{bf}(-29.867\phi_v^2 + 2.4505\phi_v + 1) \tag{4}$$

Theoretical modelling

There are different correlations to determine the tube side Nusselt number of nanofluids such as Xuan and Li correlation [18], Gnielinski correlation [5], and Dittus-Boelter correlation [19]. Xuan and Li correlation is only applicable at very low nanoparticle loadings, and it generally over predicts Nusselt number as investigated by Farajollahi *et al.* [5]. Kumar

and Sonawane [11] concluded that Gnielinski correlation provides more accurate results as compared to both Dittus-Boelter and Xuan and Li correlation. Therefore, in the current study, Gnielinski correlation for turbulent flow, given by eq. (5), was employed for the investigation of the tube side Nusselt number. The tube side Darcy friction factor was calculated using Blasius correlation [11] as given by eq. (7):

$$\mathrm{Nu_t} = 0.012(\mathrm{Re_t}^{0.87} - 280)\,\mathrm{Pr_t}^{0.4} \tag{5}$$

$$h_\mathrm{t} = \frac{\mathrm{Nu_t} k_\mathrm{t}}{D_i} \tag{6}$$

$$f_\mathrm{t} = 0.316\,\mathrm{Re_t}^{(-1/4)} \tag{7}$$

$$\Delta P_\mathrm{t} = \left(f_\mathrm{t} \frac{N_\mathrm{p} L}{2D_i} \right) \rho_\mathrm{t} u_\mathrm{t}^2 \tag{8}$$

The Bell Delaware method was employed for the calculation of shell side heat transfer coefficient as it is more accurate than other theoretical methods such as Kern and Wills-Johnston methods as discussed by Abdelkader and Zubair [20]. The eq. (9) provides heat transfer coefficient on the shells side. The ideal tube bank heat transfer coefficient, h_i, was calculated by eq. (10), while the values of correlation coefficients a_1, a_3 and a_4 were taken from Wolverine [21]. The unequal baffle spacing correction factor, J_s, was determined using eq. (11); where n is equal to 0.6 and 1/3 for turbulent flow and laminar flow, respectively:

$$h_\mathrm{s} = h_\mathrm{i}[J_\mathrm{s} J_B J_c J_\mu J_R J_L] \tag{9}$$

$$h_\mathrm{i} = \left[a_1 \left(\frac{1.33 D_i}{L_t} \right)^{\frac{a_3}{1+0.14\,\mathrm{Re}^{a_4}}} \right] \frac{j_i C_p G}{\mathrm{Pr}^{-2/3}} \tag{10}$$

$$J_\mathrm{s} = \left[\frac{(N_b - 1) + c_1^{1-n} + c_2^{1-n}}{(N_b - 1) + c_1 + c_2} \right],\ c_1 = \frac{L_\mathrm{bi}}{L_\mathrm{bc}} \text{ and } c_2 = \frac{L_\mathrm{bo}}{L_\mathrm{bc}} \tag{11}$$

The bundle bypass correction factor of the tube, J_B, was calculated using eq. (12). The value of C_bh is taken 1.25 and 1.35 for turbulent and laminar flow, respectively:

$$J_\mathrm{B} = \exp\left[-C_\mathrm{bh} \frac{L_\mathrm{bc}[D_\mathrm{s} - D_\mathrm{otl}] + L_\mathrm{pl}}{S_\mathrm{m}} \left(1 - \sqrt[3]{2 r_\mathrm{ss}} \right) \right] \tag{12}$$

$$r_\mathrm{ss} = \frac{N_\mathrm{ss}}{\frac{D_\mathrm{s}}{L_{pp}} \left[1 - 2 \left(\frac{B_\mathrm{c}}{100} \right) \right]} \tag{13}$$

The baffle cut correction factor, J_c, was determined using eq. (14). The wall viscosity correction factor is determined using eq. (16). The laminar flow correction factor is given by eq. (17):

$$J_c = 0.55 + 0.72 \left[1 - 2 \left(\frac{\theta_\mathrm{ctl}}{360} - \frac{\sin \theta_\mathrm{ctl}}{2\pi} \right) \right] \tag{14}$$

$$\theta_{\mathrm{ctl}} = 2\cos^{-1}\left[\left(\frac{D_{\mathrm{s}}}{D_{\mathrm{ctl}}}\right)\right]\left(1-\frac{2B_{\mathrm{c}}}{100}\right) \tag{15}$$

$$J_{\mu} = \left[\frac{\mu}{\mu_{\mathrm{w}}}\right]^{0.14} \tag{16}$$

$$J_{\mathrm{R}} = \left(\frac{10}{N_{\mathrm{c}}}\right)^{0.18} + \left[\left(\frac{10}{N_{\mathrm{c}}}\right)^{0.18} - 1\right]\left(\frac{20-\mathrm{Re}}{80}\right) \tag{17}$$

where

$$N_{\mathrm{c}} = \left\{N_{\mathrm{tcc}} + \frac{0.8}{L_{pp}}\left[D_{\mathrm{s}}\left(\frac{B_{\mathrm{c}}}{100}\right) - \frac{(D_{\mathrm{s}}-D_{\mathrm{ctl}})}{2}\right]\right\}(N_{\mathrm{b}}+1) \tag{18}$$

The baffle leakage correction factor, J_{L}, was calculated using eq. (19):

$$J_{\mathrm{L}} = 0.44\left(1-r_{\mathrm{s}}\right) + \left[1-0.44\left(1-r_{\mathrm{s}}\right)\right]\mathrm{e}^{-2.2r_{lm}} \tag{19}$$

where

$$r_{\mathrm{s}} = \frac{S_{\mathrm{sb}}}{S_{\mathrm{sb}}+S_{\mathrm{tb}}},\ r_{\mathrm{lm}} = \frac{S_{\mathrm{sb}}+S_{\mathrm{tb}}}{S_{\mathrm{m}}},\ S_{\mathrm{sb}} = 0.00436 D_{\mathrm{s}} L_{\mathrm{sb}} \tag{20}$$

$$S_{\mathrm{tb}} = \left[\frac{\pi}{4}\left(D_{\mathrm{t}}+L_{\mathrm{tb}}\right)^2\right]N_{\mathrm{t}}(1-F_w) \tag{21}$$

$$S_{\mathrm{m}} = L_{\mathrm{bc}}\left[L_{\mathrm{bb}} + \frac{D_{\mathrm{ctl}}}{P_{\mathrm{T,e}}}(P_{\mathrm{T}}-D_{\mathrm{t}})\right] \tag{22}$$

$$\theta_{\mathrm{ds}} = 2\cos^{-1}\left[1-2\left(\frac{B_{\mathrm{c}}}{100}\right)\right] \tag{23}$$

The overall heat transfer coefficient for the heat exchanger was determined using eq. (24):

$$\frac{1}{U} = \frac{1}{h_{\mathrm{s}}} + D_i\frac{\ln\left(\frac{D_{\mathrm{o}}}{D_{\mathrm{i}}}\right)}{2k_{\mathrm{t}}} + \frac{D_{\mathrm{i}}}{D_{\mathrm{o}}}\left(\frac{1}{h_{\mathrm{t}}}\right) \tag{24}$$

Validation of theoretical model

The theoretical model for the evaluation of thermohydraulic characteristics of ZrO_2 nanofluids, was validated by finding the overall heat transfer coefficient and pressure drop of the water. The shell side heat transfer coefficient was determined using Bell-Delaware method and tube side heat transfer was calculated using Gnielinski correlation. The results for the overall heat transfer coefficient were compared with the experimental investigation of Barzegarian *et al.* [22]. The variation in overall heat transfer coefficient with Reynolds number is shown in fig. 1. The analysis of the fig. 1 reveals that the results of Bell-Delaware method are in good agreement with the experimental results, as the maximum deviation is under 10%. So, the Bell-Delaware method can be used for the investigation of thermohydraulic characteristics of nanofluids. The validation for the pressure drop is shown in fig. 2. The comparison shows that

the results of the current study are in good agreement with the corresponding results of Sadeghinezhad *et al.* [23].

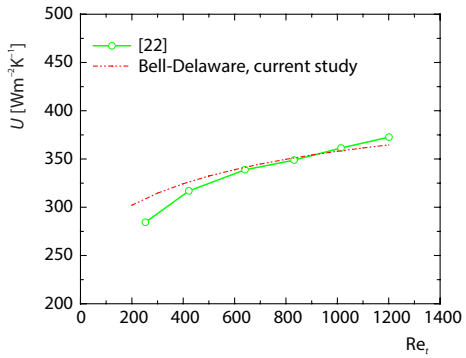

Figure 1. Comparison of the overall heat transfer coefficient with the corresponding experimental results, at a shell side mass-flow rate of 4.4 kg per minute

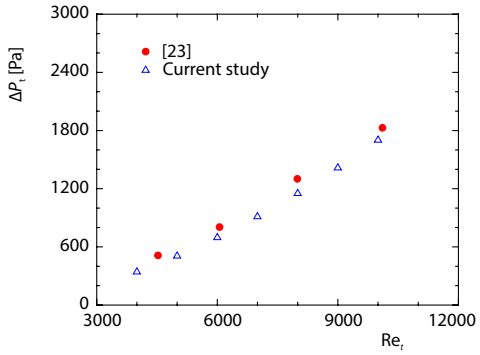

Figure 2. Comparison of the pressure drop with the corresponding investigations of Sadeghinezhad *et al.* [23]

Results

Tube side heat transfer coefficient

The influence of Reynolds number over the tube side heat transfer coefficient is indicated in fig. 3. The heat transfer coefficient has an increasing trend for all volume concentrations and a similar trend was as observed by Shahrul *et al.* [9] for water based ZnO, SiO_2, and Al_2O_3 nanofluids. The increasing rates of heat transfer coefficient are 0.807, 0.837, 0.865, 0.922 at nanoparticle concentrations of 0%, 0.2%, 0.4%, and 0.8%, respectively. A uniform augmentation in heat transfer coefficient was predicted for Reynolds number of Re = 4000-10000 at all nanoparticle concentrations. The inclusive analysis of the fig. 4. indicates that there is 3.6% increment for 0.2% ZrO_2 nanofluids, 7.2% for 0.4% ZrO_2 nanofluids, and 14.1% for 0.8% ZrO_2 nanofluids, respectively, at all Reynolds numbers. This higher heat transfer coefficient of nanofluids is perhaps due to the higher thermal conductivity of ZrO_2 nanoparticles than that of water. The experimental investigations carried by Farajollahi *et al.* [5] revealed that there was a 46% improvement in convective heat transfer coefficient for alumina nanofluids

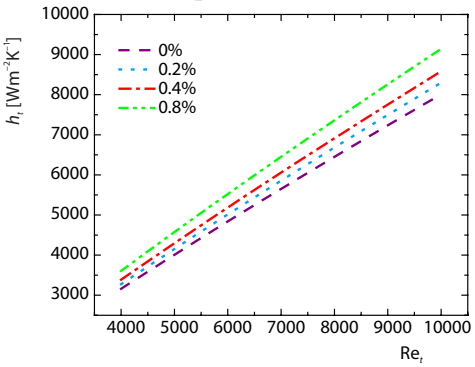

Figure 3. Tube side convective heat transfer coefficient *vs.* tube side Reynolds number for ZrO_2 nanofluids

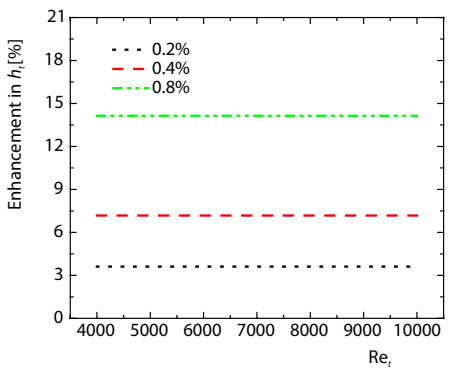

Figure 4. Enhancement in tube side convective heat transfer coefficient with tube side Reynolds number

and 56% for titina nanofluids at a volume concentration of 0.3% for both fluids. Kumar and Sonawane [11] found maximum enhancement of 20% for Fe_2O_3-water nanofluids, and 13% for Fe_2O_3-EG nanofluids at a discharge of 3 Lpm. However, in this case, the percentage augmentation in tube side convective heat transfer coefficient of ZrO_2 nanofluids is much lower than both the Al_2O_3-water and TiO-water nanofluids.

Tube side pressure drop

The tube side pressure drop of the nanofluids was calculated by considering the effects of Reynolds number and particle concentration. Also, the analysis of the heat transfer intensification using nanofluids is incomplete if the effects of enhanced viscosity of the nanofluids are not taken into account. The increased viscosity of the nanofluids results in more pressure drop, and this fact can be clearly seen in fig. 5. The pressure drop is 480.8 Pa at Re = 4000, and 2390 Pa at Re = 10,000 for volume concentration of 0.4%. Likewise, pressure drop is 911.51 Pa for 0% nanofluids, and 1747.1 Pa for 0.8% nanofluids at Reynolds number of 7000. As far as percentage enhancement in pressure drop is concerned, it increases with the increase in volume concentration but suffers insignificant variation with Reynolds number as given by fig. 6. For instance, the increase in pressure drop was 18.9%, 40.5%, and 91.6% at volume concentration of 0.2%, 0.4% and 0.8%, respectively, and at a Reynolds number of 4000.

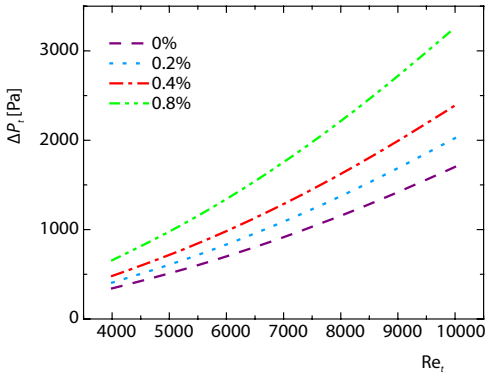

Figure 5. Tube side pressure drop *vs.* tube side Reynolds number

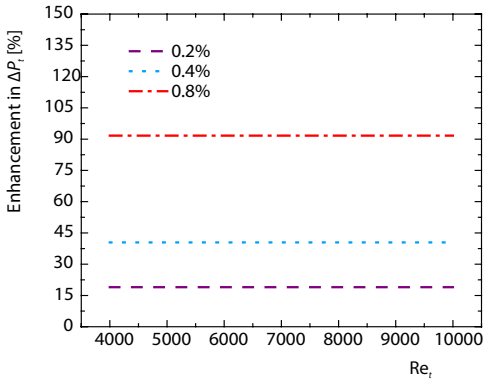

Figure 6. Enhancement in tube side pressure drop *vs.* tube side Reynolds number

Shell side heat transfer coefficient

The shell side heat transfer coefficient of the water was calculated using Bell-Delaware method. The fig. 7 depicts the effect of shell side mass-flow rate on shell side heat transfer coefficient. It is obvious from fig. 7 that the mass-flow rate has a positive effect on the shell side heat transfer coefficient, and it increases with the enhancement in shell side mass-flow rate. The shell side heat transfer coefficient increased 526.3-824.8 W/m^{2}K when the shell side mass-flow rate was increased from 4.9-11.7 kg per minute, respectively, as shown in fig. 7.

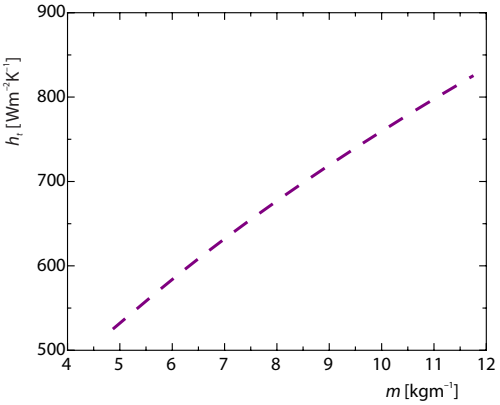

Figure 7. Shell side heat transfer coefficient *vs.* shell side mass-flow rate for water

Overall heat transfer coefficient

Figures 8-10 represents the dependence of overall heat transfer coefficient of ZrO_2-water nanofluids on different factors such as tube side Reynolds number, shell side mass-flow rate, and the tubes' configuration. The overall heat transfer coefficient increases with the increase in tube side Reynolds number, for instance, it increased from 463.2 W/m^{2}K (Re = 4000) to 498.8 W/m^{2}K (Re = 10000) for volume concentration of 0.2%.

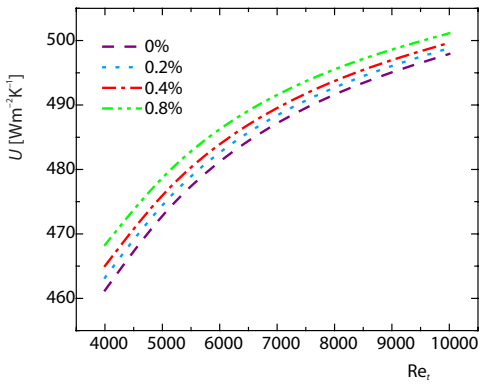

Figure 8. Overall heat transfer coefficient *vs.* tube side Reynolds number for ZrO_2 nanofluids

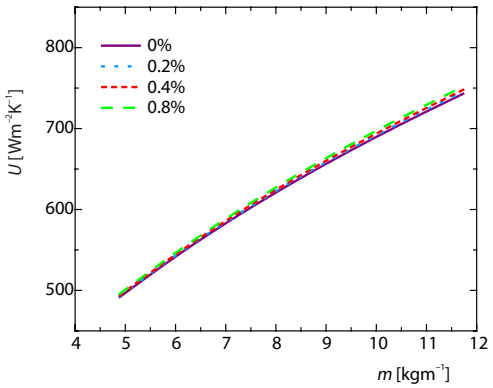

Figure 9. Overall heat transfer coefficient *vs.* shell side mass-flow rate for ZrO_2 nanofluid

In the same way, the overall heat transfer coefficient increases with the increase in volume concentration, for example, overall heat transfer coefficient was 483 W/m^{2}K for 0.2% ZrO_2-water nanofluids and it increased to 486.6 W/m^{2}K for 0.8% ZrO_2-water nanofluids at Reynolds number of 6000. However, it is important to note that the augmentation in overall heat transfer coefficient decreases with the increase in Reynolds number as revealed in fig. 10. So, it is clear that the overall heat transfer coefficient is higher on the lesser tube side Reynolds numbers. Likewise, the overall heat transfer coefficient was determined at different volume concentrations and its variation with the shell side mass-flow rate was studied. The overall heat transfer coefficient also increases with the increase in shell side mass-flow rate as shown in fig. 10. However, there is no significant improvement in overall heat transfer coefficient with the volume concentration, particularly at a lesser shell side mass-flow rate.

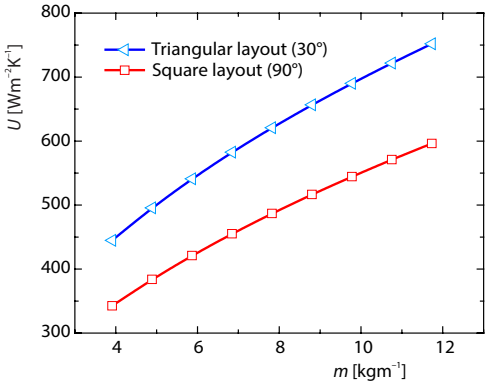

Figure 10. Overall heat transfer coefficient for different tube lay-outs different tube lay-outs

The influence of the tube arrangements on the overall heat transfer coefficient was analysed for 0.8% ZrO_2 nanofluids as depicted in fig. 10. The overall heat transfer coefficient provided by the triangular lay-out (30°) is larger than that of the square lay-out (90°). For instance, the overall heat transfer coefficient using triangular tube lay-out was 27% more than that of square lay-out at the shell side mass-flow rate of 7.8 kg/m and tube side Reynolds number of 8000 for volume concentration of 0.8%. Although the triangular lay-out provides a higher heat transfer coefficient, it accompanies with some challenges associated with the cleaning of the heat exchanger tubes.

Comparison with other nanofluids

The thermal performance of ZrO_2-water nanofluids as compared to nanofluids containing Al_2O_3, TiO_2, SiO_2, and ZnO nanoparticles is lower. For example, Farajollahi *et al.* [5] observed enhancement in overall heat transfer coefficient for H_2O-γ -Al_2O_3 and TiO_2-water nanofluids up to 16% and 24% at $\phi_v = 0.75\%$ and $\phi_v = 0.3\%$, respectively, while in the present case, the highest enhancement is 14.1% for 0.8% volume concentration for ZrO_2-water nanofluids. Similarly 12% enhancement in overall heat transfer coefficient for 0.5 vol.% SiO_2-water nanofluids, 26% for 0.5 vol.% Al_2O_3-water nanofluids, and 35% for 0.3 vol.% ZnO-water nanofluids, respectively, observed by Shahrul *et al.* [9] indicates the superiority of Al_2O_3-water and ZnO-water nanofluids over ZrO_2-water nanofluids. It may be due to the better thermophysical properties of Al_2O_3-water and ZnO-water nanofluids as compared to ZrO_2-water nanofluids. It means ZrO_2-water nanofluids are not as effective as other conventional nanofluids in heat transfer applications.

Conclusion

The thermohydraulic characteristics of ZrO_2 oxide nanofluids at low volume concentrations in a segmental baffled shell and tube heat exchanger were investigated. The effect of tube side Reynolds number was studied on tube side convective heat transfer coefficient and overall heat transfer coefficient. An improvement in tube side heat transfer coefficient was found. The convective heat transfer coefficient of the tube was increased by 3.6% for 0.2% ZrO_2 nanofluids, 7.2% for 0.4% ZrO_2 nanofluids, and 14.1% for 0.8% ZrO_2 nanofluids, respectively. The overall heat transfer coefficient was increased with the increase in tube side Reynolds number, shell side mass-flow rate and volume concentrations. However, the effect of volume concentration was less, when the variation in overall heat transfer coefficient was analysed with the shell side mass-flow rate. The triangular tube configuration provided the higher heat transfer coefficient than square tube configuration. The percentage increase in tube side pressure drop was higher as compared to percentage augmentation in tube side heat transfer coefficient. This shows that the improved heat transfer characteristics of water based ZrO_2 nanofluids are accompanied with the penalty of enhanced pressure drop.

Nomenclature

B_c – baffle cut, [–]
C_{bh} – empirical factor, [–]
C_p – specific heat, [kJkg^{-1}K^{-1}]
D_{ctl} – tube center limit diameter, [m]
D_i – tube inside diameter, [m]
D_{otl} – tube outside limit diameter, [m]
D_s – shell inside diameter, [m]
D_o – tube outside diameter, [m]
ΔP_t – tube side pressure drop, [Pa]
F_w – fraction of the cross-sectional area occupied by the window, [–]
f – friction factor, [–]
G – mass flux, [kgs^{-1}m^{-2}]
h_i – ideal tube bank heat transfer coefficient, [Wm^{-2}K^{-1}]
h_s – shell side heat transfer coefficient, [Wm^{-2}K^{-1}]
h_t – tube side heat transfer coefficient, [Wm^{-2}K^{-1}]
J_B – bundle bypass correction factor, [–]
J_c – baffle cut correction factor, [–]
J_L – baffle leakage correction factor, [–]
J_μ – wall viscosity correction factor, [–]
J_R – laminar flow correction factor, [–]
J_s – unequal baffle spacing correction factor, [–]
k – thermal conductivity, [Wm^{-1}K^{-1}]
L – length of tubes, [m]
L_{bi} – inlet baffle spacing, [m]
L_{bb} – bypass channel clearance, [m]
L_{bc} – central baffle spacing, [m]
L_{bo} – outlet baffle spacing, [m]
L_{pl} – tubes bypass lane width, [m]
L_{pp} – horizontal tube pitch, [m]
L_{sb} – diametral clearance (shell to baffle), [m]
L_{tb} – diametral tube to battle hole clearance, [m]
m – mass-flow rate, [kgs^{-1}]
N_b – number of baffles, [–]
N_c – number of tube rows, [–]

N_p – number of passes, [–]
N_{ss} – sealing strips quantity, [–]
N_{tcc} – number of tube rows per baffle section (crossed between baffle tips), [–]
Nu_t – tube side Nusselt number, [–]
Pe – Peclet number, [–]
Pr – Prandtl number, [–]
P_T – tube pitch, [m]
$P_{t,e}$ – effective tube pitch, [m]
Re – Reynolds number, [–]
r_s – ratio of areas, [–]
r_{ss} – ratio of sealing strips quantity and number of tubes in one baffle section, [–]
S_m – cross-flow area of tubes at center line, [m^2]
S_{sb} – shell to baffle leakage area, [m^2]
S_{tb} – tube to baffle leakage area, [m^2]
U – overall heat transfer coefficient, [Wm^2K^{-1}]
u – average velocity of fluid, [ms^{-1}]

Greek symbols

θ_{ctl} – baffle cut angle (relative to centerline) in degrees, [–]
θ_{ds} – baffle cut angle in degrees, [–]
ϕ – nanoparticle concentration, [–]
ρ – density of fluid, [kgm^{-3}]
μ – viscosity, [Pa·s]

Subscripts

bf – base fluid
m – mass concentration
nf – nanofluid
nm – nanoparticle
s – shell
t – tube
v – volume concentration
w – wall

References

[1] Gupta, M., *et al*., A Review on Thermophysical Properties of Nanofluids and Heat Transfer Applications, *Renewable and Sustainable Energy Reviews*, *74* (2017), July, pp. 638-670
[2] Ganvir, R. B., *et al*., Heat Transfer Characteristics in Nanofluid – A Review, *Renewable and Sustainable Energy Reviews*, *75* (2017), Aug., pp. 451-460
[3] Leong, K. Y., *et al*., Synthesis and Thermal Conductivity Characteristic of Hybrid Nanofluids – A Review, *Renewable and Sustainable Energy Reviews*, *75* (2017), Aug., pp. 868-878
[4] Ambreen, T., Kim, M.-H., Heat Transfer and Pressure Drop Correlations of Nanofluids: A State of Art Review, *Renewable and Sustainable Energy Reviews*, *91* (2018), Aug., pp. 564-583
[5] Farajollahi, B., *et al.*, Heat Transfer of Nanofluids in a Shell and Tube Heat Exchanger, *International Journal of Heat and Mass Transfer*, *53* (2010), 1-3, pp. 12-17
[6] Lotfi, R., *et al.*, Experimental Study on the Heat Transfer Enhancement of MWNT-Water Nanofluid in a Shell and Tube Heat Exchanger, *International Communications in Heat and Mass Transfer*, *39* (2012), 1, pp. 108-111
[7] Cox, J., *et al*., Application of Nanofluids in a Shell-and-Tube Heat Exchanger, *Proceedings*, ASME 2013, 11th International Conference on Nanochannels, Micro-Channels, and Minichannels, Sapporo, Japan, 2013, pp. V001T02A003
[8] Albadr, J., *et al*., Heat Transfer Through Heat Exchanger Using Al_2O_3 Nanofluid at Different Concentrations, *Case Studies in Thermal Engineering*, *1* (2013), 1, pp. 38-44
[9] Shahrul, I. M., *et al*., Experimental Investigation on Al_2O_3-W, SiO_2-W and ZnO-W Nanofluids and Their Application in a Shell and Tube Heat Exchanger, *International Journal of Heat and Mass Transfer*, *97* (2016), June, pp. 547-558
[10] Akhtari, M., *et al*., Numerical and Experimental Investigation of Heat Transfer of α-Al_2O_3/Water Nanofluid in Double Pipe and Shell and Tube Heat Exchangers, Numerical Heat Transfer – Part A: *Applications*, *63* (2013), 12, pp. 941-958
[11] Kumar, N., Sonawane, S. S., Experimental Study of Fe_2O_3/Water and Fe_2O_3/Ethylene Glycol Nanofluid Heat Transfer Enhancement in a Shell and Tube Heat Exchanger, *International Communications in Heat and Mass Transfer*, *78* (2016), Nov., pp. 277-284
[12] Haque, A. K. M. M., *et al.*, Forced Convective Heat Transfer of Aqueous Al_2O_3 Nanofluid through Shell and Tube Heat Exchanger, *Journal of Nanoscience and Nanotechnology*, *18* (2018), 3, pp. 1730-1740
[13] Shahrul, I. M., *et al*., Performance Evaluation of a Shell and Tube Heat Exchanger Operated with Oxide Based Nanofluids, *Heat and Mass Transfer*, *52* (2016), 8, pp. 1425-1433
[14] Heydari, A., *et al*., Numerical Analysis of a Small Size Baffled Shell and-Tube Heat Exchanger Using Different Nanofluids, *Heat Transfer Engineering*, *39* (2017), 2, pp. 141-153
[15] Popiel, C. O., Wojtkowiak, J., Simple Formulas for Thermophysical Properties of Liquid Water for Heat Transfer Calculations (from 0 °C to 150 °C), *Heat Transfer Engineering*, *19* (1998), 3, pp. 87-101

[16] Rea, U., *et al*., Laminar Convective Heat Transfer and Viscous Pressure Loss of Alumina-Water and Zirconia-Water Nanofluids, *International Journal of Heat and Mass Transfer*, *52* (2009), 7-8, pp. 2042-2048
[17] Li, X., *et al*., A Parametric Study of the Heat Flux Partitioning Model for Nucleate Boiling of Nanofluids, *International Journal of Thermal Sciences*, *98* (2015), Dec., pp. 42-50
[18] Xuan, Y., Li, Q., Heat Transfer Enhancement of Nanofluids, *International Journal of Heat and Fluid-Flow*, *21* (2000), 1, pp. 58-64
[19] Dittus, F. W., Boelter, L. M. K., Heat Transfer in Automobile Radiators of the Tubular Type, *International Communications in Heat and Mass Transfer*, *12* (1985), 1, pp. 3-22
[20] Abdelkader, B. A., Zubair, S. M., The Effect of a Number of Baffles on the Performance of Shell-and-Tube Heat Exchangers, *Heat Transfer Engineering*, *40* (2017), 1-2, pp. 39-52
[21] Wolverine, *Wolverine Tube Heat Transfer Data Book*, Wolverine Tube Inc., Decatur, Georgia, 1984
[22] Barzegarian, R., *et al*., Thermal Performance Augmentation Using Water Based Al_2O_3-Gamma Nanofluid in a Horizontal Shell and Tube Heat Exchanger Under Forced Circulation, *International Communications in Heat and Mass Transfer*, *86* (2017), Aug., pp. 52-59
[23] Sadeghinezhad E., *et al*., An Experimental and Numerical Investigation of Heat Transfer Enhancement for Graphene Nanoplatelets Nanofluids in Turbulent Flow Conditions, *International Journal of Heat and Mass Transfer*, *81* (2015), Feb., pp. 41-51

Paper submitted: June 15, 2018
Paper revised: September 28, 2018
Paper accepted: September 29, 2018